IDENTIFICATION OF ALTERED MINERAL USING HYPERION HYPERSPECTRAL IMAGE IN SOUTH OF TIBET, CHINA

Zhaoqiang Huang [1], *Jianchun Zheng* [2]
1. Institute of Mineral Resources, China Metallurgical Geological Bureau, Beijing 101300, China;
2. Beijing Research Center of Urban System Engineering, Beijing 100035, China;

ABSTRACT

The combination of hyperspectral data and atlas and high spectral resolution make it possible to identify altered minerals. In this paper, FLAASH atmospheric correction module and appropriate parameter settings are used to correct Hyperion hyperspectral data in Kelu deposit, Shannan area of Tibet, and then MNF conversion and anti-MNF conversion are carried out to smooth the spectrum. The ground spectrum acquired by SVC spectrometer is compared with the Hyperion result after atmospheric correction. It is considered that the Hyperion reflectance after atmospheric correction is basically consistent with the actual situation. The main altered minerals in the study area are calcite, chlorite, epidote, kaolinite and sericite by phase analysis. Then the altered minerals in the study area are identified by MTMF method, which are reliable. The result is very important meaning for mineral prospecting.

Index Terms—Kelu deposit, FLAASH, MTMF, Hyperion Hyperspectral

1. INTRODUCTION

In the early 1980s, the concept of imaging spectrometry, or hyperspectral imaging of the Earth, originated at the NASA Jet Propulsion Laboratory (JPL) (Pu et al., 2000). Imaging spectrometers acquire images in many contiguous spectral channels, which is typical to the laboratory or in situ reflectance measurements, such that for each picture element (pixel) a complete reflectance or emittance spectrum can be derived from the wavelength region covered (Goetz et al., 1985). Bandwidths and sampling greater than 25 nm rapidly lose the ability to resolve important mineral absorption features. Spectroscopy is too sensitive to small changes in the chemistry and/or structure of a material. So the narrower the spectral bandwidth, the narrower the absorption feature the spectrometer will accurately measure, if enough adjacent spectral samples are obtained (Clark, 1999). In many cases spectroscopy is very sensitive to subtle changes in crystal structure or chemistry for some materials, and spectroscopy is an excellent tool not only for detecting certain chemistries, but also at abundance levels unmatched by other tools (Clark, 1999). The reflectance spectra of ground objects provide abundant information about many important earth-surface minerals in the solar spectral range 400–2500 nm (Clark et al., 1990). So the visible near infrared (VNIR, spectral range 400-1000nm) and shortwave infrared (SWIR, spectral range 1000-2500nm) spectral range covers main spectral features of iron-bearing minerals, hydroxyl-bearing minerals, sulfates, and carbonates, such as goethite, hematite, jarosite, biotite, sericite, illite, kaolinite, montmorillonite, alunite, pyrophyllite, calcite, chlorite and epidote, et al., which are common to many geologic rock units and hydrothermal alteration assemblages(Hunt, 1977; Hunt and Ashley, 1979; Rowan et al., 2004).

The hyperspectral EO-1 Hyperion data Level 1 Gst covering Kelu area, the south of Tibet, was acquired on 1st February 2002. The image data covers the spectral range of 350–2500 nm at 10 nm bandwidth with 220 unique wavelength bands. The Hyperion Level 1 Gst product is radiometrically corrected and resampled for geometric correction and registration to a geographic map projection, and is ortho-corrected using digital elevation models (DEM) to correct parallax error due to local topographic relief, and has 242 bands. The L1G digital values represent absolute radiance values stored as 16-bit signed integers with a scaling factor of 40 for VNIR bands and 80 for SWIR bands (EO1-DFCB-0003, 2006). However, only 196 of them are calibrated such as bands 8–57 in the visible-to-near-infrared (VNIR, 426.82-925.41nm) and bands 77 to 224 in the shortwave-infrared (SWIR, 932.64 – 2395.5nm) regions, as 44 bands set to zero and two bands redundant. The Hyperion sensor has a nominal ground spatial resolution of 30 m (EO-1 User Guide, 2003). Many studies have been carried out to extract hydrothermal alteration information from volcanic and acidic sulphide systems using Hyperion hyperspectral data (Cudahy et al., 2001; Crowley et al., 2003; Kruse et al., 2003; Hubbard and Crowley, 2005; Bishop et al., 2011). This study is an attempt to use Hyperion imagery for assessing the skarn copper ore in the Kelu area, south of Tibet, where is low vegetation and adequate rock exposures.

2. GEOLOGY OF THE STUDY AREA

The Kelu study area located on Northern of Brahmaputra suture zone and South rim of the Gangdise volcano-magma arc, is underlain extensively by Cretaceous rocks of Bima

Formation, which mainly are consisted of tiny-fine limestone, metamorphic sandstone and metamorphic siltstone with marble, and partially by Cretaceous rocks of Mamuxia Formation and Tertiary rocks of Dingla Formation and Tertiary rocks of Luobusha group. Region structures mainly include EW orientation super-lithosphere fractures which result from the collision of south and north two plates, but also include the NE orientation and near SN orientation fractures which result from structure transform and include circular structures which result from magma activity and dome. Magma main rocks are intermediate-acid intrusive rocks, which include Biotite hornblende quartz monzodiorite and granodiorite and moyite and so on. Ore minerals have bornite, copper pyrite, chalcocite, cuprite, galenite and so on. The surrounding rocks alteration types are obviously zoned on both sides of the contact zone between the intermediate-acid rock mass of late Yanshanian and the Bima Formation of Lower Cretaceous-Upper Jurassic. From the contact zone to the center of the rock mass (inner contact zone), it is characterized by silicification, sericitization, epidote, chloritization, greisenization to potassium. Irregular copper polymetallic orebodies of hydrothermal altered rock type are common occurrences in the inner contact zone. From the contact zone to the stratum direction (outer contact zone), alteration is from garnet skarn, diopside garnet skarn, quartz tremolite garnet epidote skarn, silicification, limonitization, to spotted sericite hornblende. Copper-gold mineralization occurs mainly in diopside garnet epidote skarn in the outer contact zone, which is closely related to skarnization (Zhang Keyao, 2005).

3. HYPERION IMAGE AND PROCESSING

3.1. Pre-processing of the Hyperion image

The Hyperion Level 1Gst image has radiometric errors introduced by the large number of narrow and contiguous bands. So the pre-processing of Hyperion image is essential to remove the radiometric errors and acquire surface refectivity. Vertical striping, an error common to the pushbroom sensors was removed by identifying the bad bands and by replacing the bad values with the average of the good values on either side, and the integrity of spectral information was maintained, using ENVI destripe algorithm (Exelis Visual Information Solution, Inc. 2012.). Atmospheric correction and calibration to reflectance at the surface was carried out using FLAASH (Fast line-of-sight Atmospheric Analysis of Spectral Hypercubes) modules (Adler-Golden, 1998; Kruse, 2004), which would eliminate atmospheric effects through derivation of atmospheric properties such as surface albedo, surface altitude, water vapor column, aerosol, and surface and atmospheric temperatures from hyperspectral data. Minimum Noise Fraction (MNF) algorithm is usually used for segregate uncorrelated spatial noise (Green et al., 1998). The MNF bands with the calculated eigenvalue less than 1 usually do not carry useful information and mainly contains noise (Jenson, 2005). In order to eliminate noise and obtain satisfactory results, only a subset of 20 MNF-bands were maintained and then the inverse MNF was carried out to retransform the 20 MNF-bands to reflectance data. Critical atmospheric correction parameters in the FLAASH method are attributed (Table 1). Comparison between radiance curve (Fig.1) and reflectance curve (Fig.2) is done.

Table 1 Input parameters of FLAASH model atmospheric correction for the Hyperion image

Date of acquisition	GMT	Sensor altitude (km)	Ground elevation (km)	Pixel size (m)	Image center		Atmospheric model
					Lat	Lon	
2002.2.1	04:12:08	705	3.8	30	29.6638	91.5782	Mid-Latitude Summer
Water Retrieval	**Water vapour**	**Aerosol model**	**Aerosol retrieval**	**Initial visibility(km)**	**Spectral polishing**	**Width (number of bands)**	**Wavelength recalibration**
Yes	1135nm	Rural	2-band(K-T)	40	Yes	9	No
Aerosol scale height(km)	**CO2 Mixing ratio(ppm)**	**Modtran resolution**	**Modtran multiscatter model**	**Azimuth angel**	**Zenith angle**		
2.00	390.00	5cm-1	ISAACS	145.69	35.63		

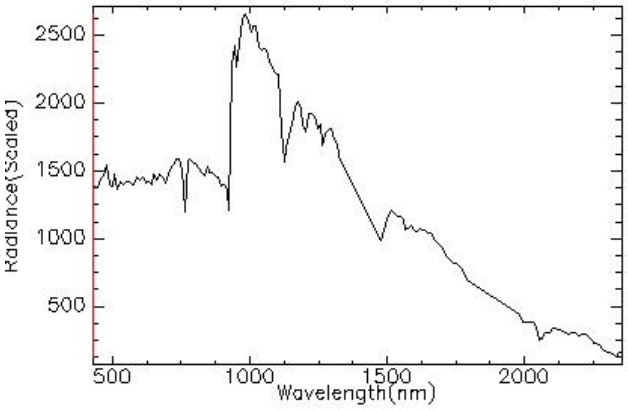

Fig.1 A sample spectral radiance of Hyperion

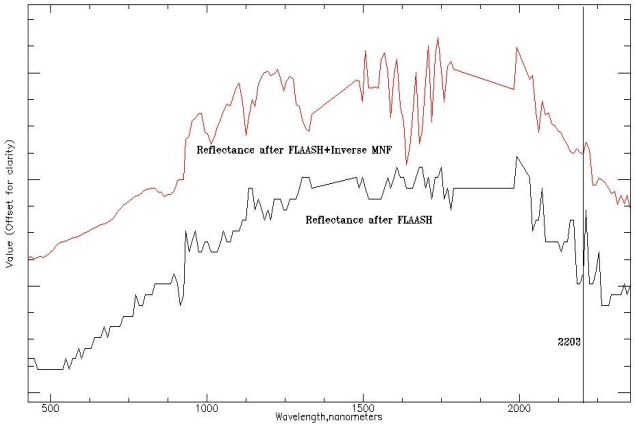

Fig.2 Comparison of Reflectance of Hyperion between FLAASH and FLAASH +Inverse MNF

3.2. Comparison between field and Hyperion image spectra

In the study area, in order to acquire information about spectral characteristics of alteration minerals, the typical rock spectra were measured by SVC field spectrometer

which has a spectral range 350-2500nm and resolution less than 2nm in range 350-1000nm, less than 4nm in range 1000-1850 and less than 3nm in range 1850-2500nm. In ENVI software, the spectra measured by SVC were resampled to Hyperion data profile using the Gaussian model. And then the comparison is done between the resampled field spectra and Hyperion spectra after FLAASH. The chloritization spectral curve of field compared with the spectral curve extracted from Hyperion image to display that two curves all have the main absorption peak 2335nm and second absorption peak 2254nm (Fig.3). The result shows that the spectral feature of the image is persisted after atmospheric correction.

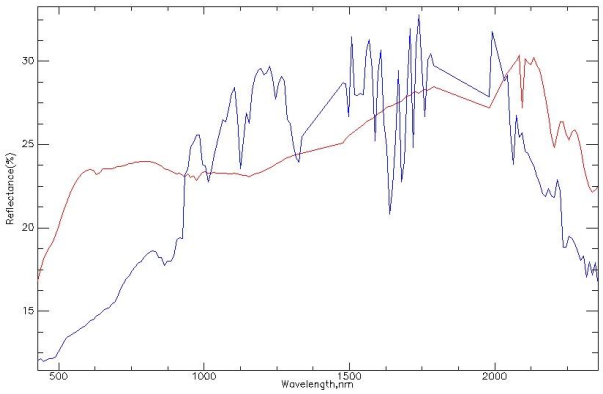

Fig.3 Comparison of SVC spectral and corresponding Hyperion reflectance

4. METHODS AND RESULTS

In order to acquire accurate altered minerals of samples, field samples were analyzed to determine their mineralogical characteristics using PANalytical X'Pert PRO MPD machine. The typical altered minerals include calcite, chlorite, epidote, kaolinite and muscovite. The mixture tuned matched filtering (MTMF, Boardman, 1998; Zadeh, 2013) method, which is a partial sub-pixel method that combines the strength of the matched filter (MF) method with the physical constraints imposed by the mixing theory, was used to unmix sub-pixel relative abundant of mineral and generate thematic mineral maps. The effectiveness of MTMF in altered mineral identification has been proved in many studies (Zadeh, 2013). Firstly, the five typical mineral spectra (Fig.4) were extracted from USGS spectral library and transformed using MNF (Green et al., 1998). And then the altered mineral matching filter (MF) maps and the infeasibility maps were generated using MTMF method. The MF maps score from 0 to 1 to estimate the relative matching between the reference spectrum and the approximate subpixel abundance. The infeasible result is based on noise sigma and shows the feasibility of MF result. Thirdly, the regions of interest of five altered minerals were delineated by 2D scatter map. The result is displayed in Fig.5. MTMF subpixel analysis, using Hyperion MNF and field sample spectra MNF results, yielded the MF scores and infeasibility bands which were used to create a 2-dimensional scatter plot. Because the most MF scores are less than 0.50, the most pixels were mixed pixels and the abundance of selected mineral is less than 50%. Regions of interest (ROI) matched to these pixels, which had high MF scores and low infeasibility, were extracted, assigned a unique color, and were overlaid a gray scale imagery. So a mineral classification map was produced with MF scores higher than zero and low infeasibility less than about 2.5 (Fig. 4).

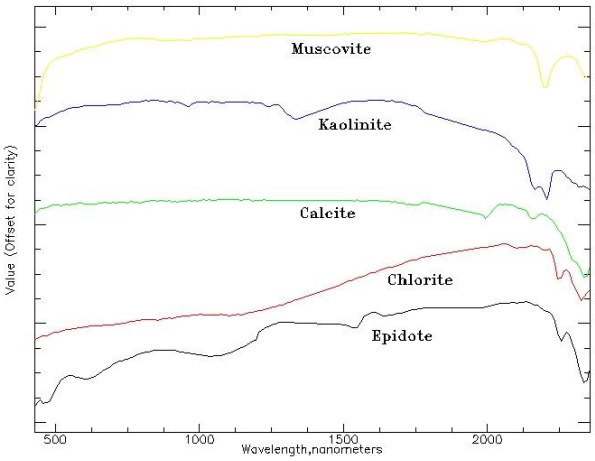

Figure 4. Five mineral spectra from USGS library

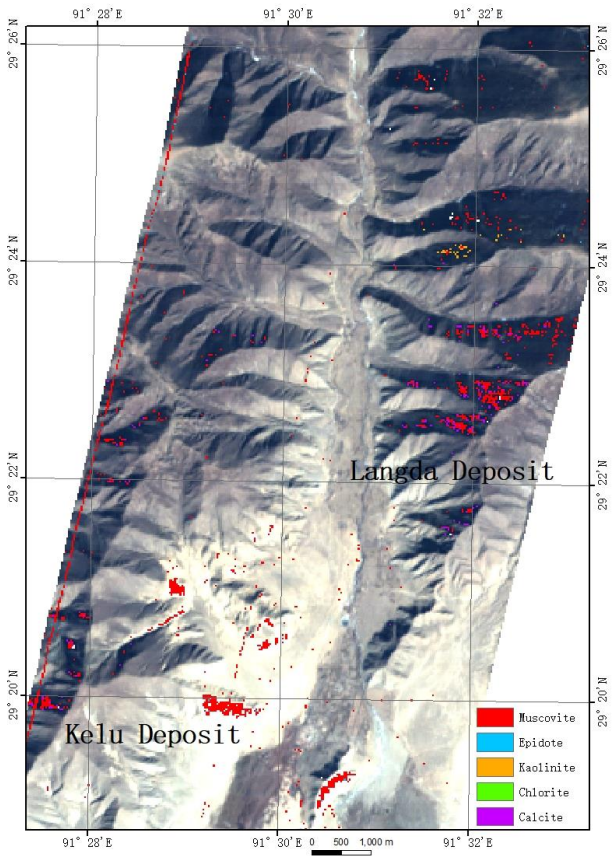

Figure 5. Mapping of Altered Mineral in Hyperion image

5. DISCUSSION AND CONCLUSIONS

The visual inspection of discriminated alteration minerals shows good correlation with the alteration maps. The study demonstrates the feasibility of using the Hyperion image data for identifying the altered mineral on skarn copper deposit in the study area after pre-processing and noise removed. And for further research the atmospheric correction is necessary to extract the true surface reflectance spectra from Hyperion image.

6. ACKNOWLEDGEMENTS

This work is supported by the National Natural Science Foundation of China (41272366) and the National Key R&D Program of China (2016YFC0600210).

7. REFERENCES

[1] Adler-Golden, S., Berk, A., Bernstein, L. S., & Richtsmeier, S.. 1998. FlAASH, A MODTRAN4 atmospheric correction package for hyperspectral data retrievals and simulations. Summaries of the seventh JPL airborne earth science workshop. JPL-Pub., vol. 97-21 (pp.1–9). Pasadena, CA: JPL Pub.

[2] Bishop, C.A., LIU, J.G., Mason, P.J., 2011. Hyperspectral remote sensing for mineral exploration in Pulang, Yunnan Province China. Int. J. Remote Sens. 32 (9), 2409 – 2426.

[3] Boardman, J.W.. 1998. Leveraging the high dimensionality of AVIRIS data for improved sub-pixel target unmixing and rejection of false positives: mixture tuned matched filtering. in: Summaries of the Seventh Annual JPL Airborne Geoscience Workshop, Pasadena, CA, 55-56.

[4] Clark, R. N., 1999. Chapter 1: Spectroscopy of Rocks and Minerals, and Principles of Spectroscopy, in Manual of Remote Sensing, Volume 3, Remote Sensing for the Earth Sciences, (A.N. Rencz, ed.) John Wiley and Sons, New York, p 3- 58.

[5] Crowley, J.K., Hubbard, B.E., Mars, J.C., 2003. Analysis of potential debris flow source areas on Mount Shasta, California, by using airborne and satellite remote sensing data. Remote Sens. Environ. 87, 345 – 358.

[6] Cudahy, T. J., Hewson, R., Huntington, J. F., Quigley, M. A., & Barry, P. S. 2002. The performance of the satellite-borne Hyperion hyperspectral VNIR-SWIR imaging system for mineral mapping at Mount Fitton, South Australia (pp.314-316). Institute of Electrical and Electronics Engineers (IEEE). https://doi.org/10.1109/igarss.2001.976142

[7] Clark, R.N., King, T.V.V., Klejwa, M., Swayze, G.A., 1990. High spectral resolution spectroscopy of minerals. Journal of Geophysical Research 95 (8), 12653–12680.

[8] EO1-DFCB-0003, HYPERION LEVEL 1GST (L1GST) PRODUCT OUTPUTFILES DATA FORMAT CONTROL BOOK (DFCB) Earth Observing-1 (EO-1). Version 1.0, April 2006. Department of the Interior U.S. Geological Survey.

[9] EO-1 User Guide, 2003. USGS Earth Resources Observation System Data Centre EDC.

[10] Exelis Visual Information Solution, Inc. 2012. ENVI Tutorial, ENVI Software Package Version 5.0

[11] Goetz, A. F. H., Vane, G., Solomon, J., Rock, B. N. 1985. Imaging spectrometry for Earth remote sensing. Science, 228, 1147−1153.

[12] Green A.A., M. Berman, P. Switzer, M.D. Craig. 1998. A transformation for ordering multispectral data in terms of image quality with implications for noise removal. IEEE Transactions on Geoscience and Remote Sensing, 26:65-74.

[13] Hubbard, B., Crowley, J.K., 2005. Mineral mapping on the Chilean – Bolivian Altiplano using co-orbital ALI, ASTER and Hyperion imagery: data dimensionality issues and solutions. Remote Sens. Environ. 99 (1 – 2), 173 – 186.

[14] Hunt, G.R., 1977. Spectral signatures of particulate minerals in the visible and near infrared. Geophysics 42, 501 – 513.

[15] Hunt, G.R., Ashley, P., 1979. Spectra of altered rocks in the visible and near infrared. Econ. Geol. 74, 1613 – 1629.

[16] Jenson, J.R., 2005. Introductory Digital Image Processing. A Remote Sensing Perspective. Pearson, Prentice Hall, Upper Saddle River.

[17] Kruse, F. A.. 2004. Comparison of ATREM, ACORN, and FLAASH atmospheric corrections using low-altitude AVIRIS data of Boulder, CO. Summaries of 13th JPL Airborne Geoscience Workshop, Jet Propulsion Lab, Pasadena, CA.

[18] Kruse, F.A., Boardman, J.W., Huntigton, J.F., 2003. Comparison of airborne Hyperspectral data and EO-1 Hyperion for mineral mapping. IEEE Trans. Geosci. Remote Sens. 41 (6), 1388 – 1400, IEEE Aerospace Conference Proceedings.

[19] PU Ruiliang, GONG Peng. 2000. Hyperspectral Remote Sensing and Applications. Beijing: Higher Education Press.

[20] Rowan, L.C., Simpson, C.J., Mars, J.C., 2004. Hyperspectral analysis of the Ultramafic complex and adjacent Lithologies at Mordor, NT, Australia. Remote Sens. Environ. 91, 419 – 431.

[21] Zadeh, H. M., Tangestani, M.H., Velasco Roldan, F., Yusta, I., 2013. Mineral exploration and alteration zone mapping using mixture tuned matched filtering approach on ASTER data at the central part of Dehaj-Sarduiyeh copper belt SE Iran. IEEE Sel. Top. Appl. Earth Obs. Remote Sens.. http://dx.doi.org/10.1109/JSTARS.2013.2261800.

[22] Zhang Keyao. 2005. Study on the Predict ion of the Ore-f inding Target of the Keru Cuproaurite in Zhanang County, Tibet. Geology of Fujian, 24(2), 65-71.